

Seismic analysis of liquid metal reactor piping systems*

Work performed under the auspices of the US Department of Energy, by a contractor of the US Government under contract No. W-31-109-ENG-38. Accordingly, the US Government retains a nonexclusive, royalty free license to publish or reproduce the published form of this contribution, or allow others to do so, for US Government purposes.

C.Y.Wang

Reactor Analysis and Safety Division, Argonne National Laboratory,
Argonne, Illinois 60439 USA

CONF-870812--13

CONF-870812--13

Received by OSM

DE87 011400

JUL 9 6 1987

1 INTRODUCTION

An important concern in the safety analysis of liquid metal reactors (LMRs) is the structural integrity of piping systems subjected to seismic events and other abnormal conditions such as thermal transients and pressure-wave propagations. Under such conditions, excessive deformations and distortions of piping components could occur which may cause plastic deformation as well as possible structural damage to the system.

To safely assess the adequacy of the LMR piping, a three-dimensional piping code, SHAPS [1-2], has been developed at Argonne National Laboratory. This code was initially intended for calculating hydrodynamic-wave propagation in a complex piping network. It has salient features for treating fluid transients of fluid-structure interactions for piping with in-line components. The code also provides excellent structural capabilities of computing stresses arising from internal pressurization and 3-D flexural motion of the piping system. As part of the development effort, the SHAPS code has been further augmented recently by introducing the capabilities of calculating piping response subjected to seismic excitations.

This paper describes the finite-element numerical algorithm and its applications to LMR piping under seismic excitations. A time-history analysis technique using the implicit temporal integration scheme is addressed. A 3-D pipe element is formulated which has eight degrees of freedom per node (three displacements, three rotations, one membrane displacement, and one bending rotation) to account for the hoop, flexural, rotational, and torsional modes of the piping system. Both geometric and material nonlinearities are considered. This algorithm is unconditionally stable and is particularly suited for the seismic analysis.

2 NUMERICAL ALGORITHM

The present implicit structural module in the SHAPS code permits the

*Work performed under the auspices of the US Department of Energy, Office of Technology Support Programs, under contract W-31-109-ENG-38

MASTER

Seismic analysis of liquid metal reactor piping systems

C.Y.Wang

DISTRIBUTION OF THIS DOCUMENT IS UNLIMITED

9/8/87

analysis of larger piping systems for longer durations. This is especially useful in the seismic analyses of piping systems where the seismic excitation may last for many seconds. Two approaches have been incorporated into the SHAPS code. One solves the displacement and stress fields with respect to the global coordinate systems and another provides displacement and stress solution relative to supports where acceleration histories are input. Support points can have the same or different acceleration input along any or all of the three translational axes.

To illustrate the analysis, we present here the governing equation of seismic analysis in which the displacement field is obtained relative to supports with reference accelerations. For the convenience of developing the implicit-integration algorithm, let us rewrite the global equations of motion in the form

$$(1) \quad [M] \{A_{n+1}\} + \{F^{int}(D_{n+1})\} + [C] \{v_{n+1}\} = \{F^{ext}\} ,$$

where $[M]$, $\{A\}$, $\{F^{int}\}$ and $\{F^{ext}\}$ denote the global mass matrix, nodal accelerations, and nodal internal and external forces, respectively. The subscript $n+1$ denotes the advanced-time cycle. Also, we should mention that the internal nodal force $\{F^{int}\}$ is a function of nodal displacements in the advanced-time cycle; $[C]$ is the damping matrix. Based on the method of linearization, the nodal internal force at the advanced-time iteration can be expressed as a function of previous iteration values [2]

$$(2) \quad \{F^{int}(D_{n+1}^{i+1})\} \approx \{F^{int}(D_{n+1}^i)\} + [K(D_{n+1}^i)] \{\Delta D\} + \dots ,$$

where $[K]$ is the global stiffness matrix; superscripts $i+1$ and i are the current and previous iterations, respectively. The damping matrix $[C]$ sometimes can be written as

$$(3) \quad [C] = \bar{\alpha} [M] + \bar{\beta} [K] ,$$

where $\bar{\alpha}$ and $\bar{\beta}$ are proportional constants.

Denoting input reference accelerations and the corresponding velocities by $\{\bar{a}\}$ and $\{\bar{v}\}$, we have

$$(4) \quad \{A_{n+1}\} = \{\bar{a}_{n+1}\} + \{a_{n+1}\}$$

and

$$(5) \quad \{v_{n+1}\} = \{\bar{v}_{n+1}\} + \{v_{n+1}\}$$

in which $\{a\}$ and $\{v\}$ represent accelerations and velocities relative to supports with prescribed motion. From Newmark- β formula [3] the relative displacements, accelerations, and velocities have the form

$$(6) \quad \{d_{n+1}^{i+1}\} = \{d_{n+1}^i\} + \{\Delta d\} ,$$

$$(7) \quad \{a_{n+1}^{i+1}\} = [\{d_{n+1}^i\} + \{\Delta d\} - \{d_n\} - \Delta t \{v_n\} \\ - (0.5-\beta)\Delta t^2 \{a_n\}] \beta \Delta t^2 ,$$

$$(8) \quad \{v_{n+1}^{i+1}\} = \{v_n\} + (1-\gamma)\Delta t \{a_n\} + \gamma \Delta t \{a_{n+1}^{i+1}\} .$$

In Eqs. (6)-(8), β and γ are the integration constants. Substituting Eqs. (2)-(8) into Eq. (1), and after certain rearranging, the resulting equation yields

$$(9) \quad [K^*] \{\Delta d\} = \{\Delta F^*\}$$

where

$$(10) \quad [K^*] = [M] + \beta \Delta t^2 [K] + \gamma \Delta t (\bar{\alpha}[M] + \bar{\beta}[K]) ,$$

$$(11) \quad \{\Delta F^*\} = \beta \Delta t^2 \left(\{F_{n+1}^{\text{ext}}\} - \{F_{n+1}^{\text{int}}\}^i - [M] \{\bar{a}_{n+1}\} \right. \\ \left. - (\bar{\alpha}[M] + \bar{\beta}[K]) \{\bar{v}_{n+1}\} \right) - \left[[M] + \gamma \Delta t (\bar{\alpha}[M] + \bar{\beta}[K]) \right] \\ \left[\{d_{n+1}^i\} - \{d_n\} - \Delta t \{v_n\} - \left(\frac{1}{2} - \beta \right) \Delta t^2 \{a_n\} \right] \\ - \beta \Delta t^2 \left(\bar{\alpha}[M] + \bar{\beta}[K] \right) \left[\{v_n\} + (1-\gamma) \Delta t \{a_n\} \right] .$$

Equation (9) is solved at each time step to obtain the relative displacement increment $\{\Delta d\}$. The new relative displacements, accelerations, and velocities are then found from Eqs. (6), (7), and (8). Note that the effective force $\{\Delta F^*\}$ consists of the reference accelerations and velocities $\{\bar{a}_{n+1}\}$ and $\{\bar{v}_{n+1}\}$, which can be directly obtained through input as well as the time-integration procedure.

3 SAMPLE CALCULATION

To demonstrate the capability of SHAPS code in analyzing the piping structural response generated from seismic excitation, a three

dimensional complex piping system subject to a seismic excitation of 6-s duration is presented. The mathematical model given in Fig. 1 represents the hog-leg piping connecting the IHXs and primary pump. The finite-element model consists of seven pipes and six elbows which were further discretized by 78 elements. In the analysis, each elbow is modeled by four segmented pipe elements. The piping system has a constant O.D. of 61.4 cm and a thickness of 1.27 cm. The input acceleration shown in Fig. 2 is a scaled version of the El Centro earthquake acceleration time history with a maximum acceleration of 0.484 g at 3.71 s. This acceleration history was applied at two end points of the piping loop in the horizontal or global X direction. Fluid mass and piping insulation are included in the analysis to realistically simulate the prototypical condition. The entire piping system is supported at two end points connecting to the IHX and pump, as well as at two intermediate points (nodes 27 and 53) where no vertical motion is allowed.

Relative displacements in the X-direction at all midpoints of pipes and elbows are obtained. Figures 3-5 present the displacement time histories and Fourier spectra at nodes 24, 40, and 56 of pipes 3, 4, and 5, respectively. The maximum displacement is about 0.5 cm. The corresponding characteristic frequencies are obtained through a fast Fourier transform (FFT) frequency generating subroutine. Results reveal that the piping system has two dominant frequencies. The first one is about 2.67 Hz, generating from the transverse vibration of the first pipe (adjacent to the IHX) which is perpendicular to the X-direction. The second one is about 9.6 Hz, originating from the longitudinal oscillation of the last pipe (next to the primary pump) which is parallel to the X-direction. We have found from the results that the dominant frequency of each node depends on its associated pipe orientation. For instance, at nodes 24 and 56 where pipe is parallel to the seismic excitation, the dominant frequencies are due to longitudinal oscillation of the last pipe, and have values of 9.6 and 9.17 Hz, respectively. On the other hand, at node 40 where pipe is perpendicular to the X-direction, the dominant frequency is about 2.67 Hz.

This computer run consists of 1200 cycles with a constant time step of 0.005 s. The CPU time for the numerical calculation is 37 minutes; the cost is about \$40.00, based upon the weekend discount rate. The above information thus demonstrates the efficiency of the SHAPS code in calculating the piping seismic response.

REFERENCES

Wang, C.Y. 1982. A Three-Dimensional Method for Integrated Transient Analysis of Reactor-Piping Systems, Nuclear Engineering and Design, 66 (2), 175-184.

Wang, C.Y. & W.R. Zeuch 1986. An Advanced Multi-Dimensional Method for Structural and Hydrodynamic Analysis of LMFBR Piping Systems, Nuclear Science and Engineering, 92 (1), 170-177.

Newmark, N.M. 1959. A Method of Computation for Structural Dynamics, Journal of Engineering Mechanics Division of American Society of Civil Engineers, 85, 67-94.

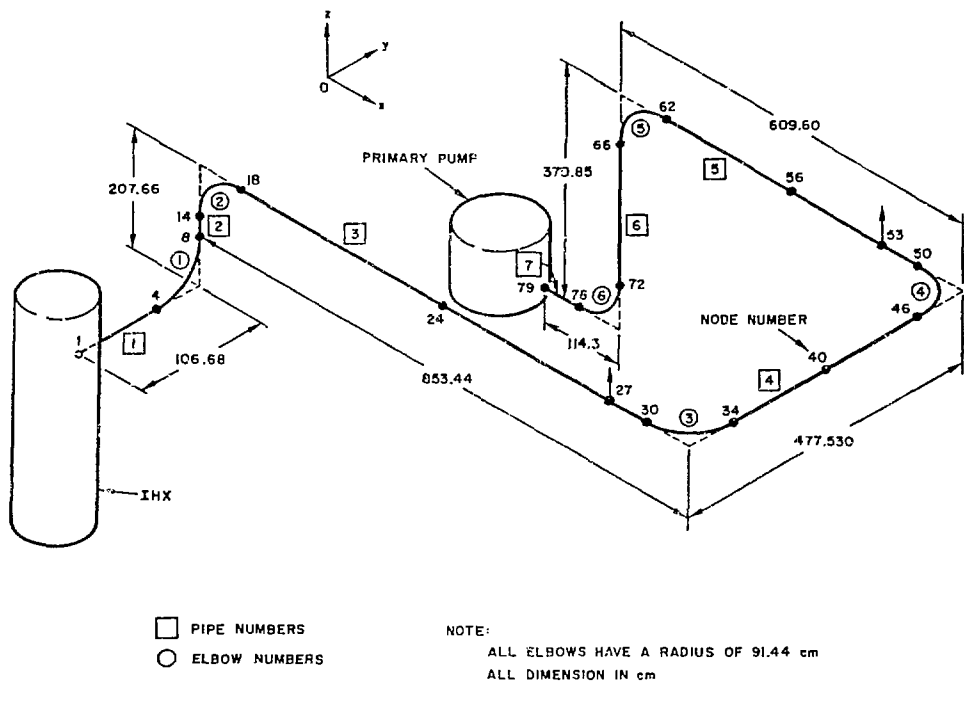


Figure 1. Mathematical Model of a LMR Hot-Leg Piping Loop

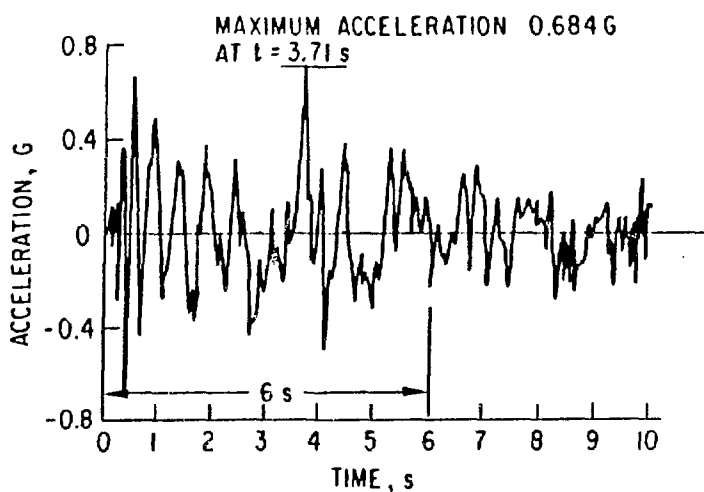


Figure 2. Acceleration - Time History of Support Motions

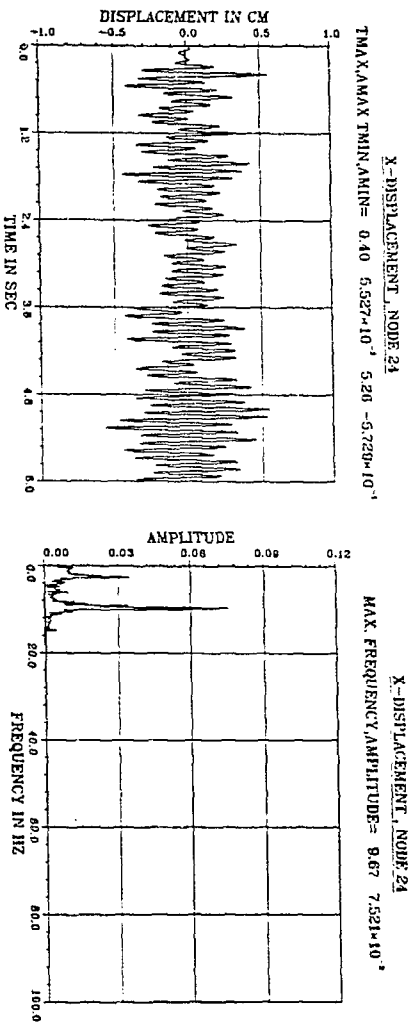


Figure 3. X-Displacement and Fourier Spectrum at Node 24

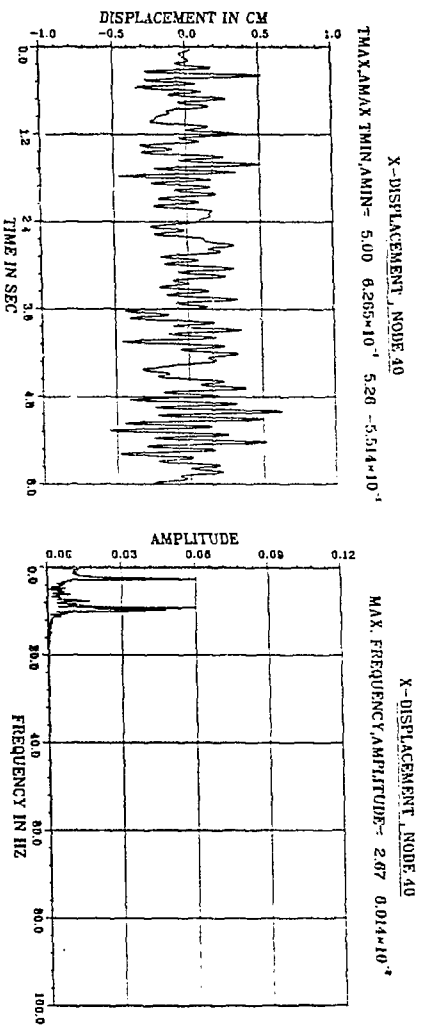


Figure 4. X-Displacement and Fourier Spectrum at Node 40

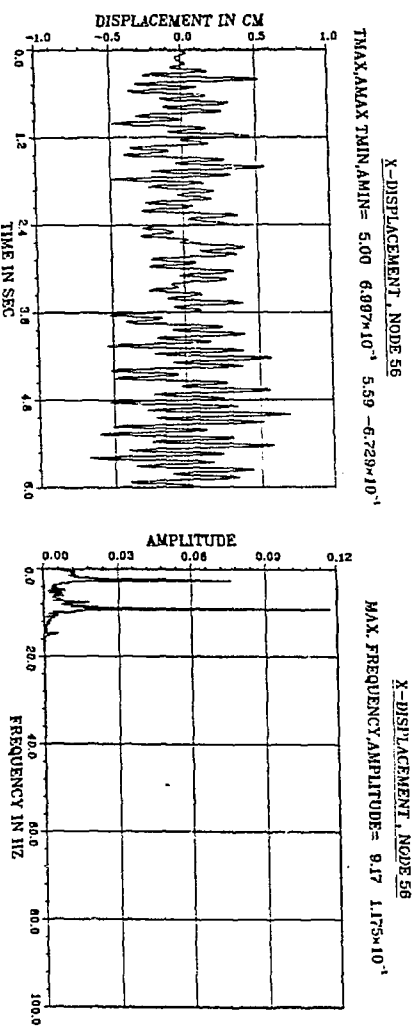


Figure 5. X-Displacement and Fourier Spectrum at Node 56

DISCLAIMER

This report was prepared as an account of work sponsored by an agency of the United States Government. Neither the United States Government nor any agency thereof, nor any of their employees, makes any warranty, express or implied, or assumes any legal liability or responsibility for the accuracy, completeness, or usefulness of any information, apparatus, product, or process disclosed, or represents that its use would not infringe privately owned rights. Reference herein to any specific commercial product, process, or service by trade name, trademark, manufacturer, or otherwise does not necessarily constitute or imply its endorsement, recommendation, or favoring by the United States Government or any agency thereof. The views and opinions of authors expressed herein do not necessarily state or reflect those of the United States Government or any agency thereof.